https://dx.doi.org/10.1016/j.apor.2020.102200

Cyclic volumetric strain accumulation for sand under drained simple shear condition

Ze-Xiang WU[a], Zhen-Yu YIN[b,c,*], Christophe DANO[d], Pierre-Yves HICHER[e]

Affiliations:

[a] Collage of Architecture and Civil Engineering, Wenzhou University, Wenzhou, China

[b] Southern Marine Science and Engineering Guangdong Laboratory (Guangzhou), 1119 Haibin Rd., Nansha District, Guangzhou, China

[c] Department of Civil and Environmental Engineering, The Hong Kong Polytechnic University, Hung Hom, Kowloon, Hong Kong

[d] University Grenoble Alpes, CNRS, Grenoble INP, 3SR, Grenoble, France

[e] Research Institute of Civil Engineering and Mechanics (GeM), UMR CNRS 6183, Ecole Centrale de Nantes, Nantes 44321, France

[*] Corresponding author: Dr Zhen-Yu Yin, Tel. +852 34008470, Fax +852 23346389, E-mail: zhenyu.yin@polyu.edu.hk; zhenyu.yin@gmail.com

Abstract: Volumetric strain of a soil element surrounding the pile accumulated under the drained cyclic loading condition is one of major concerns in geotechnical engineering design. In this paper, twenty stress-controlled drained simple shear tests, with 5000 cycles on Fontainebleau sand have been carried out, which aims to investigate four factors influencing cyclic accumulation behaviour: initial void ratio, normal stress, cyclic shear stress ratio and average shear stress ratio. Based on results, the cyclic volumetric strain accumulation for each influencing factor is summarized, which is found highly sensitive to the cyclic shear stress ratio that a bigger magnitude (more than 0.2) leads to a larger degree of densification. In addition, a simple analytical model is then proposed accounting for these factors with seven parameters that can be directly calibrated from laboratory tests. Finally, the applicability of the model is examined by simulating the additional tests through an adoption of the parameters calibrated by the training tests.

Keywords: Cyclic behaviour; simple shear; strain accumulation; sand; analytical model

1 Introduction

During long-term cyclic loading, because of cyclic strain accumulation in the soils surrounding piles, the serviceability of a pile foundation will be adversely affected. According to the Mohr-Coulomb criterion, the mobilised shear stress acting on the pile shaft depends on the level of the radial effective stress applied to the soil-pile interface [1-3], meaning that any change in the radial effective stress or strain caused by cyclic loading will greatly affect the bearing capacity of the pile foundation. Hence, to explain the basic mechanisms of pile resistance under cyclic loading, a large number of field and/or laboratory-based model pile cyclic loading tests have been performed over the past few decades. For example, Jardine and Standing [4, 5] demonstrated that a high level of cyclic loading is highly detrimental to shaft capacity, based on their experimental results on an in-situ pile test being subjected to a large amount of axial cyclic loading. More recently, Tsuha et al. [6] and Rimoy [7] presented a series of reduced-scale cyclic tests, using the mini-Imperial College pile (ICP), that demonstrated the cyclic degradation of radial stresses adjacent to the pile. All cyclic pile tests show that the shaft capacity depends on the mechanical response of a soil element (strain or excess pore pressure accumulation) adjacent to a pile under cyclic loading [8-11]. Thus, it is of great importance to study the cyclic behaviour of the soil element around the pile.

In a laboratory elementary test, to obtain high-quality and reliable data, in-situ conditions should be replicated as closely as possible. Three general types of laboratory equipment, with easily operable features, have been widely used to study the soil element's behaviour around the pile, including triaxial tests, direct interface shear tests and simple shear tests to simulate the field constructions [12-17]. Recently, the cyclic behaviour of soils has been widely studied via triaxial tests [18-22]. However, without the principal stress rotation, the real shearing state of soils adjacent to the pile still cannot be adequately replicated [23], which utterly restricts its

application to shaft degradation. Moreover, Boulon and Foray [24] suggested that the constant normal stiffness condition can reproduce the interface pile-loading boundary conditions. Following this proposition, Pra-ai and Boulon [25] performed a series of cyclic constant normal stiffness direct interface shear tests with a large number of cycles, to investigate the progressive degradation of normal effective stress. The constant normal stiffness tests were performed by continually adjusting the values of normal stress and strain respectively by keeping the ratio of normal stress to strain constant. However, the value of normal stiffness depends on the sample depth (through the pressuremeter modulus) and the pile radius, which also limits its general application.

Comparing it against triaxial tests and direct shear tests, Anderson [26] pointed out that the simple shear test has been acknowledged to provide more representative loading conditions for shearing of soils adjacent to a pile, such as that the cyclic shear strain develops more symmetrically than triaxial tests and can also take into account the principal shear rotation during the shear process corresponding to piles under axial cyclic loading. A large number of undrained or constant volume cyclic simple shear tests have been conducted to investigate the cyclic responses of soils, including liquefaction, degradation of both shear stiffness and the damping ratio, and effective normal stress [27-30]. Recently, different types of laboratory tests have also been performed on various sands considering the effects of size/shape characteristics on the cyclic responses of sands [31-37]. In addition, the behaviour of strain accumulation in sand has been already examined considering the influences of amplitude, relative density and normal stress based on different types of tests [38-42]. Moreover, a detailed parametric study about simple shear tests has also been performed by Duku et al. [43], but only considering low number of cycles ($N \leq 50$). Although these models have their advantages, the coupling effects of different initial conditions on volumetric strain cannot be well described, and the strain-related cyclic response has received less discussion. An empirical model to describe the cyclic

78 strain accumulation behaviour considering different influences (e.g. initial void ratio or relative
79 density, normal stress, cyclic shear stress ratio and average shear stress ratio) remains unclear
80 because of a lack of relevant tests, although it is considered an important impact factor for the
81 analysis of shaft capacity [18, 44-46].

82 The aim of this paper is to analyse the volumetric strain accumulation in sand specimens
83 through cyclic simple shear tests under constant normal stress condition. A series of drained
84 cyclic simple shear tests is first performed on Fontainebleau sand, which includes four initial
85 states with different factors: (1) initial void ratios, (2) initial normal stresses, (3) cyclic shear
86 stresses and (4) average shear stresses. Moreover, the experimental results are also interpreted
87 to summarise the relationships between volumetric strain accumulation and each factor. Finally,
88 the development of an analytical model, to predict the cyclic accumulation of volumetric strain,
89 is expounded, taking into account the effect of the initial void ratio, initial normal stress, cyclic
90 shear stress and average shear stresses.

91 # 2 Experimental investigation

92 ## 2.1 Material and simple shear apparatus

93 Fontainebleau sand NE34, a geotechnical reference material in France, widely used in
94 cyclic triaxial tests [20, 47-49] and direct shear tests [25], was adopted for this study. The tested
95 sand is a kind of fine siliceous sand with sub-rounded grains, a roundness of R = 0.390 and a
96 sphericity of S = 0.749 [50]. Its main characteristics are summarized in Table 1 [48, 51].

97 Table 1 Physical properties of Fontainebleau sand NE34

S_iO_2: %	D_{50}(mm)	$C_u(D_{60}/D_{10})$	G_s	e_{max}	e_{min}
99.70	0.21	1.53	2.65	0.882	0.510

98

The simple shear tests were conducted using a commercial device (GDS-simple shear apparatus) whose design is close to the NGI simple shear apparatus [52, 53]. The servo-controlled system (as seen in Figure 1) is capable of conducting stress/strain controlled in both horizontal and vertical directions. The stress path of soil element adjacent to a pile can be performed by controlling the vertical and horizontal boundaries on the specimen in the GDS simple shear apparatus, which correspond to radical and shaft directions in the soil surrounding the pile respectively[46].

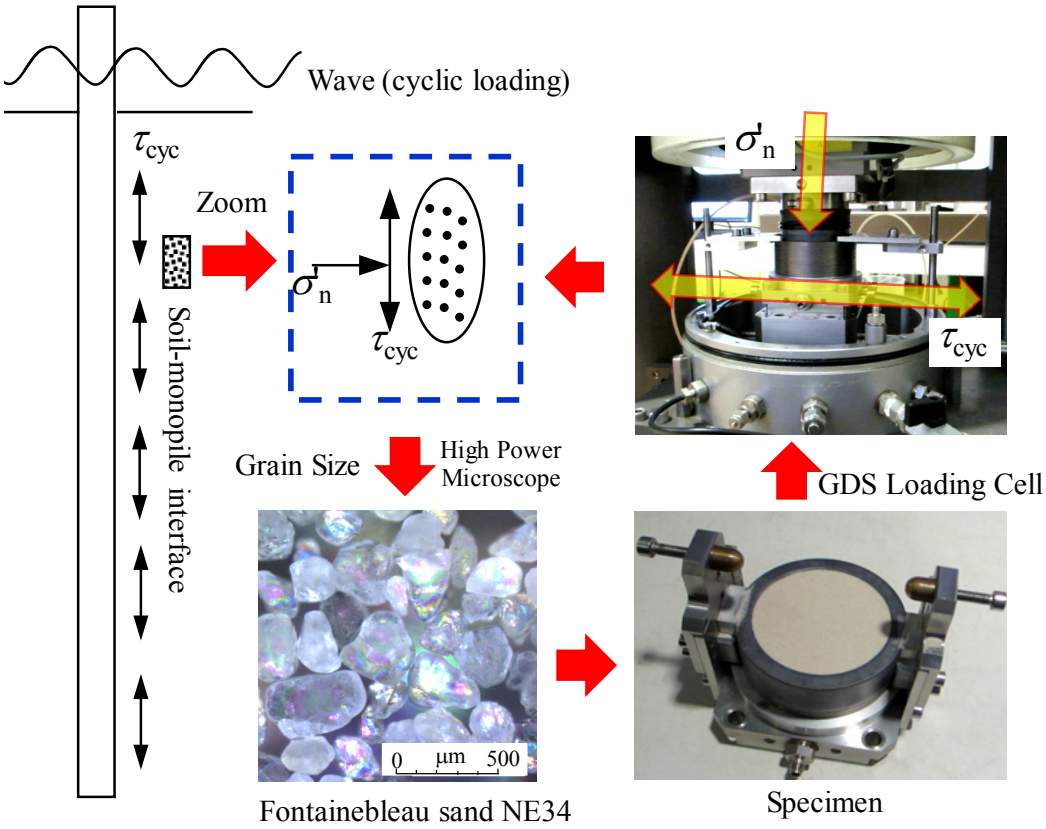

Figure 1 Analysis of soil element based on simple shear apparatus

The cylindrical reconstituted specimens with a size of 70 mm in diameter and 25 mm in height (ratio of 0.36 to minimize the effects of friction on the lateral sides), were prepared by air-pluviation method using dry sand, which is considered to approximate the natural deposition process [54]. The dry sand was pluviated out of a funnel into the mould, at the same time the funnel was continuously lifted up in order to keep a constant distance between the

outlet of the funnel and the sand surface in the mould. The specimen was confined in a soft butyl membrane with 0.2 mm thickness, itself placed against a stack of rigid rings (with 1 mm thin each) which maintains a constant cross-sectional area. On both sides, the sand is in contact with rough sintered stainless-steel plates to prevent any sliding between the top/bottom pedestals and the specimen. Note that the behaviours of dry sand and fully saturated sand are generally considered identical [55, 56].

During the axial cyclic loading of pile, the effective normal stress σ'_n in soil surrounding the pile will be firstly reduced due to the cyclic accumulation of volumetric strain in contraction (according the simple theory of stress-strain $\sigma=E\cdot\varepsilon$). Then, the lateral shear stress acting on the pile shaft τ_f is decreased following the simple Coulomb failure criterion ($\tau_f=\sigma'_n\cdot\tan(\phi_f)$ where ϕ_f represents the friction angle of sand). Meanwhile, the external shaft capacity obtained by integrating τ_f over the external pile area is degraded, resulting in a decrease of the bearing capacity of the pile. Therefore, the study of modelling the accumulation of volumetric strain is applicable to judge the degradation of bearing capacity of piles under cyclic axial loading.

2.2 Testing program

The drained simple shear testing was ensured by constraining a constant effective normal stress σ'_n on the dry specimen after K_0-consolidation (or compression under one-dimensional (1D) condition), noted that this stage took two hours, then followed by the cyclic shearing stage immediately. The cyclic shear motion, inducing a cyclic shear stress τ_{cyc}, was generated by the displacement of the bottom pedestal, while the top one was horizontally fixed. For cyclic loading, sine cycles with a frequency of 0.2 Hz were applied which is close to the predominant wave frequency applying to the offshore wind turbine system ranging from 0.1 Hz to 0.3 Hz[46, 57]. The volumetric strain $\varepsilon_v = \Delta H/H_c$ was measured by the change of the specimen height

138 (ΔH) during the cyclic process over the height after 1D compression (H_c). According to the
139 experimental results with large number of cycles (e.g. 10^4 to 10^6), the volumetric strain
140 gradually accumulates in the first 5000 cycles and then tends to be stable during cyclic loading
141 [18, 40, 46, 58]. Therefore, Therefore, to focus on investigating the initial accumulation part
142 of deformation development of the specimen under stress-controlled cyclic simple shearing
143 condition, 5000 cycles were selected for all tests.

144 To investigate the effects of different initial states and propose a general analytical model
145 for calculating the volumetric strain accumulation, a total of 20 tests were conducted, as shown
146 in Table 2. In order to reproduce the real state of soil around the pile, these tests can be divided
147 into four groups as follows: (1) different initial void ratio e_0 (No. 1–4) reflecting the initial
148 shear contraction/dilation behaviour; (2) different initial normal stress σ'_n (No. 2, 5–7)
149 corresponding to the soil around the pile at different depths; (3) different cyclic stress ratio
150 CSR = τ_{cyc}/σ'_n (No. 8–12) and (4) different average stress ratio $\alpha = \tau_{ave}/\sigma'_n$ (No. 2, 13–15)
151 corresponding to the combined cyclic stress state of the surrounding soil with different average
152 stresses. In addition, other tests (No. 16–20), with initial states that extended from those of the
153 first 15, were conducted to validate the analytical model.

154 Table 2 Experimental program of cyclic simple shear tests

No.	e_i	e_0	D_{r0} /%	D_r /%	σ'_n /kPa	τ_{cyc} /kPa	τ_{ave} /kPa	α	CSR	N
1	0.697	0.668	49.7	57.6	416	41.6	0	0	0.1	5000
2	0.651	0.628	62.1	68.2	416	41.6	0	0	0.1	5000
3	0.592	0.568	78.0	84.3	416	41.6	0	0	0.1	5000
4	0.559	0.539	86.8	92.2	416	41.6	0	0	0.1	5000
5	0.646	0.623	63.4	69.7	52	5.2	0	0	0.1	5000
6	0.649	0.627	62.6	68.5	104	10.4	0	0	0.1	5000
7	0.650	0.619	62.4	70.5	208	20.8	0	0	0.1	5000
8	0.640	0.604	65.1	74.8	416	41.6	0	0	0.1	5000
9	0.635	0.606	66.4	74.3	416	50.0	0	0	0.12	5000

10	0.641	0.609	64.8	73.4	416	83.2	0	0	0.2	5000
11	0.635	0.601	66.4	75.4	416	104.0	0	0	0.25	5000
12	0.639	0.605	65.3	74.3	416	133.1	0	0	0.32	5000
13	0.650	0.628	62.4	68.2	416	41.6	20.8	0.05	0.1	5000
14	0.650	0.631	62.4	67.5	416	41.6	41.6	0.1	0.1	5000
15	0.650	0.629	62.4	67.8	416	41.6	83.2	0.2	0.1	5000
16	0.737	0.703	39.0	48.2	416	41.6	0	0	0.1	5000
17	0.552	0.536	88.7	93.4	416	41.6	0	0	0.1	5000
18	0.649	0.604	62.6	74.7	416	20.8	0	0	0.05	5000
19	0.639	0.606	65.3	74.2	416	166.4	0	0	0.4	5000
20	0.650	0.629	62.4	67.8	416	41.6	124.8	0.3	0.1	5000

Noted: e_i is the initial void ratio; e_0 is void ratio after 1D compression; D_{r0} is initial relative density; D_r is relative density after 1D compression.

2.3 Cyclic densification

Based on the experimental results, the cyclic responses of specimens were first studied by plotting the stress-strain paths, as seen in Figure 2. Four groups of cyclic volumetric strain accumulation behaviour were summarized, as follows:

1) For different relative densities D_r after 1D compression (Figure 2 a-b), the stress-controlled cyclic shearing condition will lead to unsymmetrical accumulation of shear strain γ, and the looser sand corresponds to a larger level of shear strain accumulation as well as of densification;
2) For different normal stress levels σ'_n (Figure 2 c-d), with the increase in the initial normal stress σ'_n, the magnitude of shear strain accumulation rises and also produces a larger level of densification for sand;
3) For different cyclic shear stress ratios (CSR) (Figure 2 e-f), it may be observed that the shear strain γ and void ratio e are highly sensitive to the amplitude of cyclic shear stress τ_{cyc}, in which a greater magnitude of CSR will lead to greater shear strain accumulation as well as a larger degree of densification, especially in the initial five

cycles;

4) For different average shear stress ratios α (Figure 2 g-h), an increase in average shear stress will promote the accumulation of shear strain γ and restrain the magnitude of densification.

Overall, cyclic tests reveal that the volumetric strain is regularly accumulated during cyclic loading, and that it is possible to formulate the volumetric strain accumulation based on different effects (see details of the parametric study in Section 3).

The shear strain accumulation also occurs under the stress controlled cyclic simple shearing. As seen in Figure 2, the shear strain has been gradually accumulated, since the direction of the loading into the first quarter of the cycle, in which the direction of accumulation is still keeping along the direction of started cyclic loading. Furthermore, the amplitude of shear strain depends on the magnitude of cyclic shear stress (τ_{cyc}) where bigger shear stress results in bigger shear strain amplitude, as shown in the Figure 2 (d and f). In addition, the magnitude of shear strain amplitude decreases significantly with increasing the number of cycles during the first 100 cycles, and then trends to be stable.

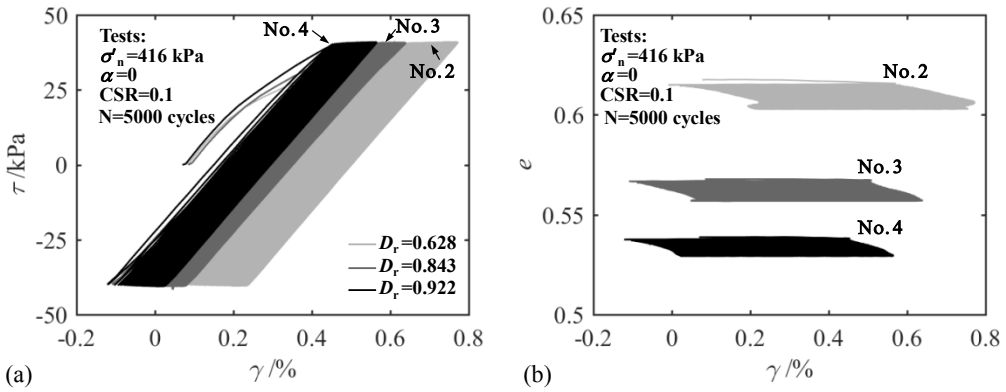

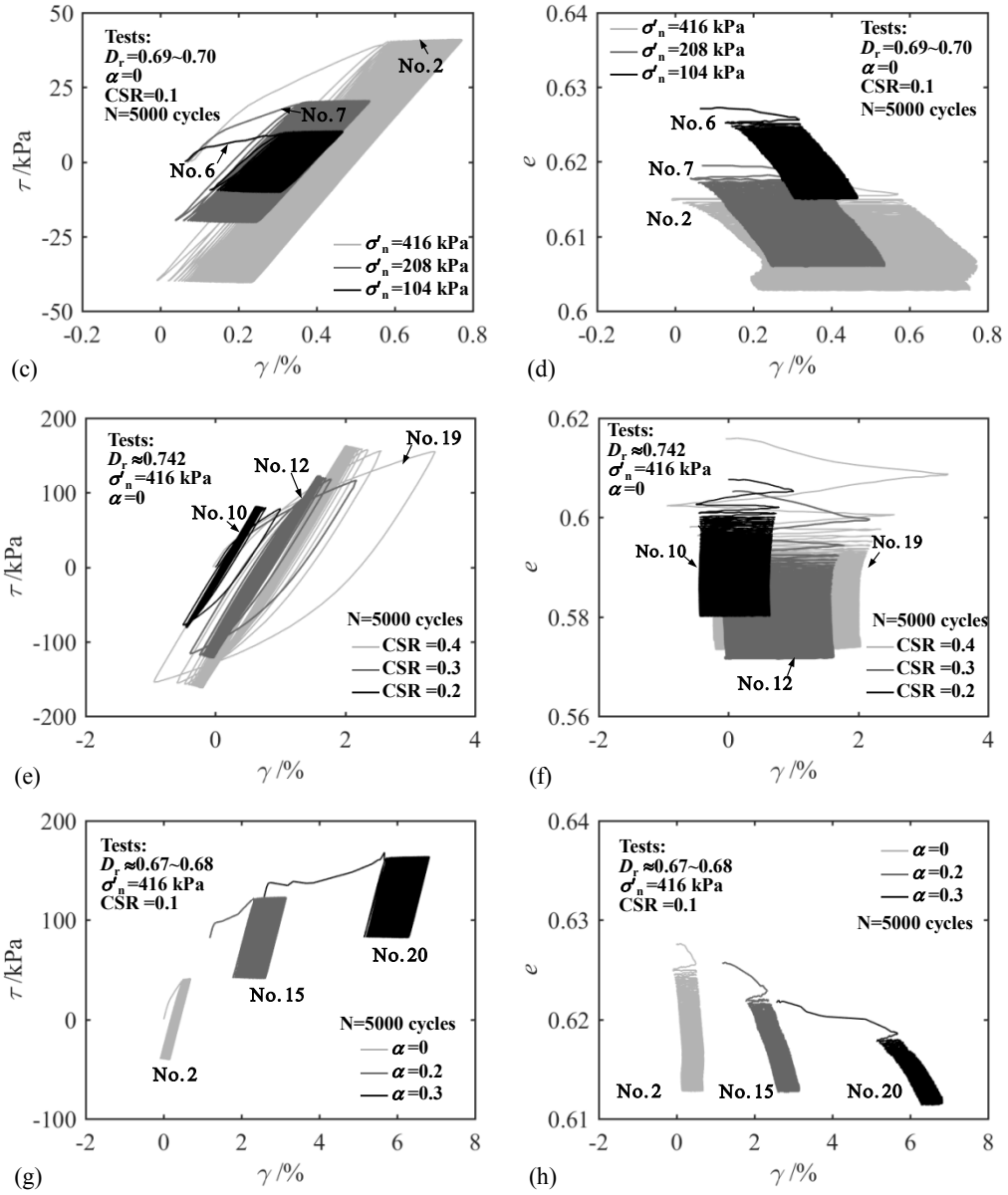

Figure 2 Summary of drained cyclic simple shear results: (a)-(b) comparisons by different initial relative densities; (c)-(d) comparisons by different effective normal stresses; (e)-(f) comparisons by different cyclic shear stress ratios and (g)-(h) comparisons by different average shear stress ratios.

3 Interpretation of experimental results

3.1 Effect of relative density

The effect of the relative density D_r, varying from 0.576 to 0.922 on strain accumulation ε_v, was studied, based on tests (No. 1–4) with constant cyclic shear stress and normal stress. Figure 3 (a) demonstrates that sand with a lower relative density has a higher strain

202 accumulation, while Figure 3 (b) presents the volumetric strains ε_v against the relative density
203 D_r for selected numbers of cycles corresponding to N = 3, 10, 100, 1000, 2000 and 5000
204 respectively. Conventionally, the positive volumetric strain is for describing contractive
205 behaviour and the negative volumetric strain is for describing dilative behaviour. This shows
206 that the accumulated volumetric strain ε_v decreases linearly with the increase in relative density
207 for each selected number in the double logarithmic coordinates, which can be expressed as:

208 $$\frac{\varepsilon_v}{\varepsilon_{v-D_r}^{ref}} = \left(\frac{D_r}{D_r^{ref}} \right)^{C_1} \tag{1}$$

209 where C_1 is the slope of the curve in the double-logarithmic plot (C_1=-0.8); this can be
210 considered as the same for different numbers of cycles. For convenience, the reference relative
211 density is considered as $D_r^{ref} = 1$. Then six reference volumetric strains $\varepsilon_{v\text{-}D_r}^{ref}$ at $D_r^{ref} = 1$ in
212 Figure 3 (b) can be obtained for six selected numbers of cycles N, which is plotted in Figure 3
213 (c). The initial values of volumetric strain at zero number of cycles were due to the stage of
214 initial 1D compression. Based on this linear relationship, the reference volumetric strain can
215 be expressed by:

216 $$\varepsilon_{v-D_r}^{ref} = n_1 \log\left(N+1\right) \tag{2}$$

217 in which n_1 is the slope of the curve in the semi-logarithmic plot (n_1=0.0017), with null
218 volumetric strain at zero number of cycles. In Figure 3 (a), the volumetric strain is plotted from
219 the first cycle (N=1) in the logarithmic coordinate system.

220 Substituting Eq. (2) in Eq. (1), the volumetric strain, evolving with the number of cycles
221 and considering the effect of initial density, is finally expressed by:

222 $$\varepsilon_v = n_1 D_r^{C_1} \log\left(N+1\right) \tag{3}$$

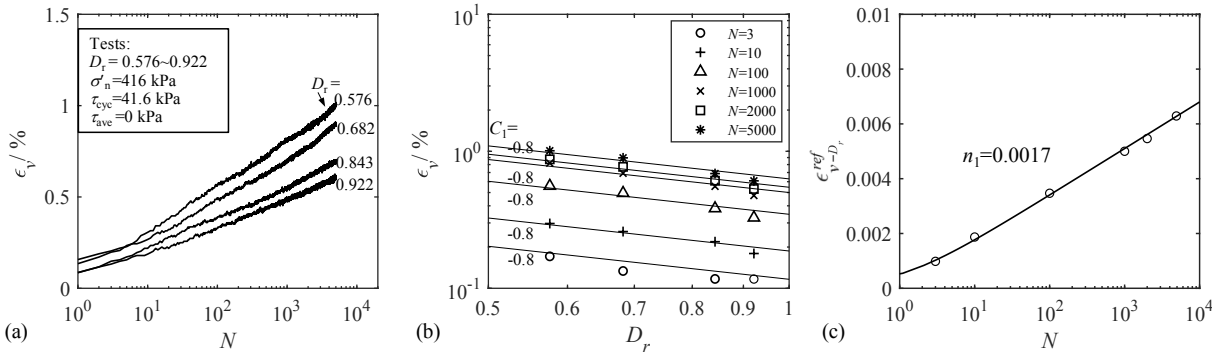

Figure 3 Volumetric strain accumulation with different relative densities: (a) volumetric strain versus number of cycles; (b) volumetric strain versus relative density; (c) reference volumetric strain versus number of cycles

3.2 Effect of normal stress level

The effect of the normal stress on strain accumulation, varying from 52 to 416kPa, was studied with a constant cyclic stress ratio (CSR = 0.1) and relative density (D_r = 0.68~0.7) based on tests (No. 2, 5–7). Figure 4(a) shows that sand with a higher normal stress corresponds to a higher volumetric strain accumulation; Figure 4 (b) presents the volumetric strains ε_v versus the ratio of normalised normal stresses and atmospheric pressure (p_{at} = 100kPa) in each selected number of cycles, corresponding to N = 2, 10, 100, 1000, 2000 and 5000 respectively. This shows that the accumulated volumetric strain ε_v increases linearly with the increase in normal stress for each selected number, which can be expressed as:

$$\frac{\varepsilon_v}{\varepsilon^{ref}_{v-\sigma'_n}} = \left(\frac{\sigma'_n}{p_{at}}\right)^{C_2} \tag{4}$$

where C_2 is the slope of the curve in a double-logarithmic plot (C_2 = 0.18), which can be considered similar for different numbers of cycles. Six reference volumetric strains $\varepsilon^{ref}_{v-\sigma'_n}$ at $\sigma'_n = p_{at}$ in Figure 4 (b) can be obtained for six selected numbers of cycles N.

Figure 4 (c) presents the relationship between the reference volumetric strain and the number of cycles N in semi-logarithmic coordinates, which can be expressed by:

$$\varepsilon_{v\text{-}\sigma'_n}^{ref} = n_2 \log\left(N+1\right) \tag{5}$$

where n_2 is the slope of the curve in a semi-logarithmic plot with null volumetric strain at zero number of cycles (n_2 = 0.0008). The evaluation of volumetric strain with number of cycles, considering the effect of normal stress, can ultimately be expressed as follows,

$$\varepsilon_v = n_2 \left(\frac{\sigma'_n}{p_{at}}\right)^{C_2} \log\left(N+1\right) \tag{6}$$

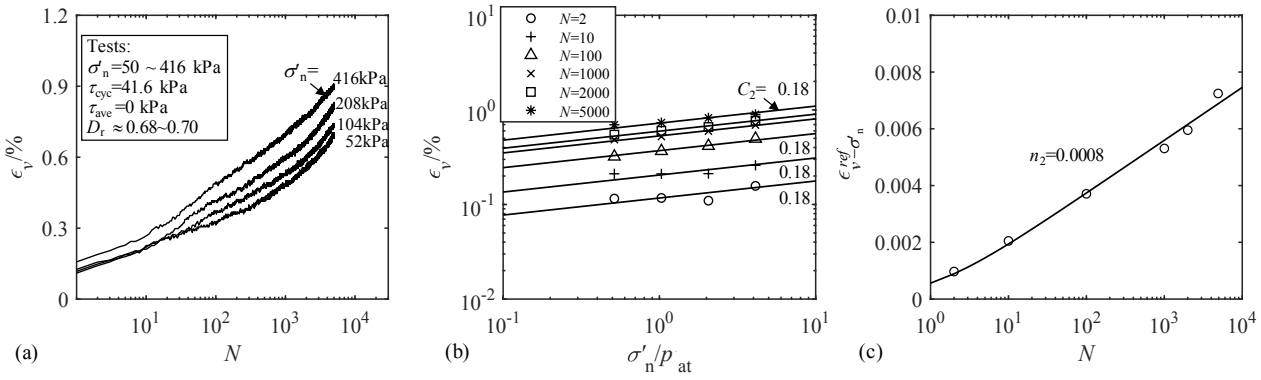

Figure 4 Volumetric strain accumulation with different normal stress level: (a) volumetric strain versus number of cycles; (b) volumetric strain versus normal stress level; (c) reference volumetric strain versus number of cycles

3.3 Effect of cyclic shear stress ratio

The effect of CSR (= τ_{cyc}/σ'_n) on volumetric strain ε_v, varying from 0.1 to 0.32, was studied based on tests (No. 8–12) with constant normal stress (σ'_n = 416kPa), null average shear stress and constant relative density (D_r = 0.73~0.75). Figure 5(a) shows that sand with a higher cyclic stress ratio corresponds to a higher rate of cyclic volumetric strain accumulation. To minimise the effects of normal stress and relative density, the volumetric strain ε_v was first normalised by the density-related function (Eq. (1)) and normal stress-related function (Eq. (4)), as shown in Eq. (7). Then, the normalized volumetric strain $\overline{\varepsilon_v}$ could be used to compare the cases between different CSRs (noted that all tests (No. 8–12) have performed with the same normal

stress level, the normalization of minimize the effects of normal stress is not necessary in this case.

$$\overline{\varepsilon}_v = \frac{\varepsilon_v}{D_r^{C_1} \cdot \left(\sigma'_n / p_{at}\right)^{C_2}} \tag{7}$$

Figure 5 (b) shows the normalised volumetric strains $\overline{\varepsilon}_v$ versus the CSR for selected numbers of cycles, corresponding to N = 3, 10, 100, 1000, 2000 and 5000, respectively, in which selecting the normalized volumetric strain $\overline{\varepsilon}_v$ (Eq. (7)) as y-axis is to reduce the effects of relative density and initial normal stress. This denotes that the relationship between normalised volumetric strains and CSRs for a selected cyclic number can be expressed as follows:

$$\overline{\varepsilon}_v = C_3 \cdot CSR^{\varepsilon_{v\text{-}CSR}^{ref}} \tag{8}$$

where C_3 is a constant (C_3 = 0.031), and the slope corresponds to the volumetric strain related state parameter $\varepsilon_{v\text{-}CSR}^{ref}$, which representing the change in the normalized volumetric strain with changes in the cyclic stress ratio. Six reference volumetric strains related state parameter $\varepsilon_{v\text{-}CSR}^{ref}$ were plotted against the selected numbers of cycles N in Figure 5 (c), which can be expressed by Eq.(9):

$$\varepsilon_{v\text{-}CSR}^{ref} = C_4 \cdot \left(N\right)^{C_5} \tag{9}$$

where C_4 and C_5 are CSR-related parameters obtained by fitting the curve (C_4 = 1.715 and C_5 = -0.1).

The normalized accumulated volumetric strain, taking into account the effect of CSR, can finally be derived by substituting Eq. (9) into Eq. (8), as follows:

$$\overline{\varepsilon}_v = C_3 \cdot CSR^{C_4 \cdot (N)^{C_5}} \tag{10}$$

Thus, the accumulated volumetric strain accounting for the effects of soil density, normal stress level and CSR can be obtained by substituting Eq. (10) into Eq. (7),

$$\varepsilon_v = D_r^{C_1} \cdot \left(\sigma'_n / p_{at}\right)^{C_2} \cdot C_3 \cdot CSR^{C_4 \cdot (N)^{C_5}} \tag{11}$$

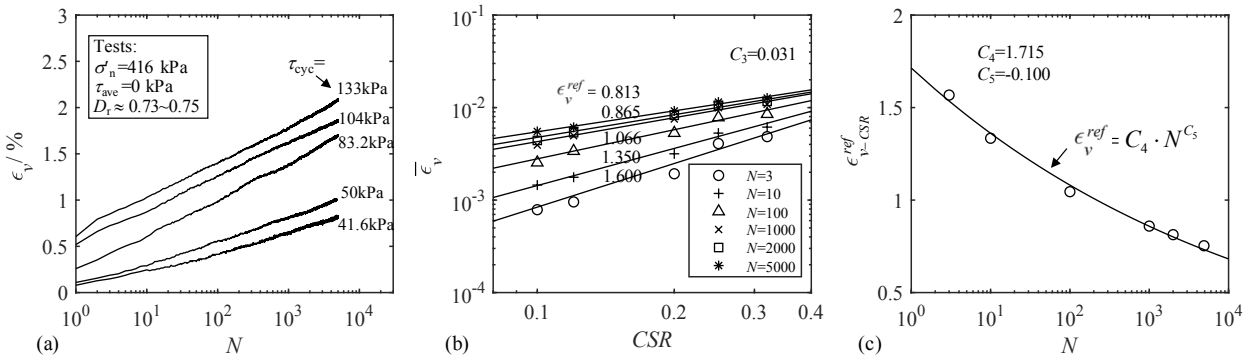

Figure 5 Volumetric strain accumulation with different cyclic stress ratio: (a) volumetric strain versus number of cycles; (b) normalized volumetric strain versus cyclic shear stress ratio; (c) reference volumetric strain versus number of cycles

3.4 Effect of average shear stress ratio

The effect of the average shear stress ratio α (= τ_{ave}/σ'_n) on volumetric strain ε_v, varying from 0 to 0.2, was studied based on tests (No. 2, 13–15) with constant normal stress and CSR. The initial average shear stress is reached in drained condition. Figure 6 (a) shows that sand with a higher average shear stress corresponds to a lower rate of volumetric accumulation. Figure 6 (b) presents the normalised volumetric strains $\overline{\varepsilon}_v$ calibrated by Eq. (7) versus the average stress ratio, in the selected numbers of cycles corresponding to N = 2, 10, 100, 1000, 2000 and 5000. The accumulated, normalised volumetric strain $\overline{\varepsilon}_v$ can be expressed by Eq. (12):

$$\overline{\varepsilon}_v = \left(\overline{\varepsilon}_v\right)_{\alpha=0} + \varepsilon_{v-\alpha}^{ref} \cdot \alpha \tag{12}$$

where $\left(\bar{\varepsilon}_v\right)_{\alpha=0}$ is the accumulated volumetric strain for the case with zero average shear stress expressed by Eq. (10). The volumetric strain related state parameter $\varepsilon_{v\text{-}\alpha}^{ref}$ corresponds to the change in the normalized volumetric strain with the changes in the average shear stress ratio. This shows that the slope decreases from positive to negative with the increase in numbers of cycles.

Figure 6 (c) presents the relationship between the six reference volumetric strains related state parameter $\varepsilon_{v-\alpha}^{ref}$ and the selected numbers of cycles *N*, which can be fitted by the linear expression in semi-logarithmic coordinates, per Eq. (13):

$$\varepsilon_{v-\alpha}^{ref} = C_6 \log\left(N+1\right) + C_7 \tag{13}$$

where C_6 and C_7 are average shear stress ratio-related parameters (C_6 = -0.0013 and C_7 = 0.0043). Substituting Eq. (13) into Eq. (12), the volumetric strain, evolving with the number of cycles and considering the effect of average shear stress, is finally expressed as follows:

$$\bar{\varepsilon}_v = C_3 \cdot CSR^{C_4 \cdot (N)^{C_5}} + \alpha\left[C_6 \log\left(N+1\right) + C_7\right] \tag{14}$$

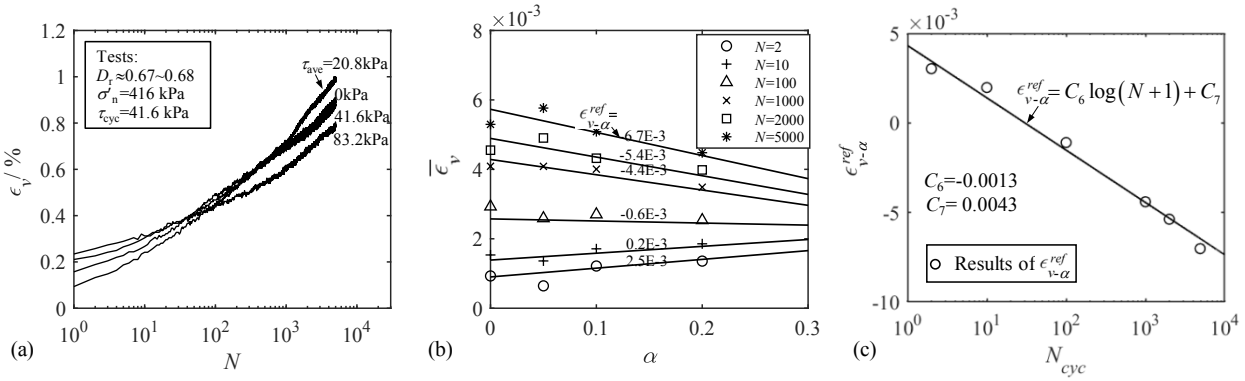

Figure 6 Volumetric strain accumulation with different average shear stress ratio: (a) volumetric strain versus number of cycles; (b) normalized volumetric strain versus average shear stress ratio; (c) reference volumetric strain versus number of cycles

3.5 Final analytical model

All above experimental investigation demonstrates that the cyclic volumetric strain accumulation depends on four key factors: relative density, normal stress level, CSR and average shear stress ratio. Four reference strains ($\varepsilon_{v\text{-}D_r}^{ref}$, $\varepsilon_{v\text{-}\sigma'_n}^{ref}$, $\varepsilon_{v\text{-}CSR}^{ref}$ and $\varepsilon_{v\text{-}\alpha}^{ref}$) have no physical meaning, and can be eliminated during formula derivation. Overall, a general analytical model can be derived by substituting Eq. (14) into Eq. (7), as follows:

$$\varepsilon_v = D_r^{C_1}\left(\frac{\sigma'_n}{p_{at}}\right)^{C_2}\left[C_3 \cdot CSR^{C_4 \cdot N^{C_5}} + \alpha\left(C_6 \ln\left(N+1\right)+C_7\right)\right] \tag{15}$$

The Eq. (15) for the volumetric strain consists of two summands. The first summand describes the volumetric strain accumulation affected by the cyclic shear stress ratio *CSR*, while the second summand captures the effect of the average shear stress ratio α. As the boundary, zero CSR gives zero of the first summand, and a non-zero α of the second summand at N=0 still gives volumetric strain "$\alpha \bullet C_7$" which is mobilized during shear (i.e. shear stress dilatancy).

4 Calibration and validation

Based on above interpretations, all input parameters of the analytical model are summarised in Table 3, which can be calibrated by using training tests as shown in Figures 3-6. To show the performance of the proposed analytical model, the previous training tests were selected to replicate the volumetric strain accumulation during cyclic loading, as shown in Figure 7. Through comparison of the experimental results in Figures 3-6, it is shown that the calculated curves are in good agreement with experimental results. Moreover, the basic characteristics of volumetric strain accumulation, considering all these effects, can be summarised as follows:

1) For different relative densities (D_r) with CSR = 0.1, the accumulation ratio gradually decreases with the increase in density (Figure 7(a)).

2) The effect of the initial normal stress σ'_n is similar to the effect of relative densities (D_r); that is, the accumulation ratio gradually rises with increasing normal stress (Figure 7(b)).

3) For CSRs, a greater value will produce a larger accumulation from the first cycle to the subsequent 5000 cycles, which means that the volumetric strain is highly sensitive to the CSR throughout the cyclic process (Figure 7(c)).

4) For the average shear stress τ_{ave}, higher value of τ_{ave} results initially in a higher volumetric strain, but gives a smaller evolution of volumetric strain with the number of cycles (Figure 7(d)).

Furthermore, five additional tests (No. 16–20) with different initial density, cyclic shear stress ratio and average shear stress ratio from the previous first 15 training tests were simulated, using the calibrated parameters, to verify the applicability of the analytical method. A good agreement between the predictions and experiments can be found in Figure 8, which indicates that the analytical model can successfully describe the cyclic responses in terms of volumetric strain.

Figure 9 presents the experimental results regarding evolution of the volumetric strain with cyclic loading from 10 to 5000 cycles, based on six groups including different combinations of the key factors D_r, σ'_n, CSR and α. The volumetric strain surfaces, as calculated by the analytical model, were first plotted in conjunction with the experimental results to evaluate the combined effects in multi-dimensional space.

According to the six groups' results, we may see that, with increasing cyclic numbers, the calculated volumetric strain-related surface gradually enlarges along the axis of volumetric strain and gradually shrinks along the axis of the average shear stress ratio α. The most sensitive combined-effects group is a combination of D_r and CSR, as shown in Figure 9 (b), in which

366 the surface enlarges rapidly and forms a highly steep slope along both the D_r and CSR
367 directions. In addition, the least sensitive combined-effects group is the combination of D_r and
368 σ'_n, as seen in Figure 9 (f) where the volumetric strain surface is enlarged almost in parallel
369 with the cyclic number.

370 Table 3 Summary of the empirical function with parameters of Fontainebleau sand

Function	Parameters	
D_r related function $f_{den} = \left(D_r / D_r^{ref}\right)^{C_1}$	C_1	-0.8
σ'_n related function $f_{nor} = \left(\sigma'_n / p'_{at}\right)^{C_2}$	C_2	0.18
CSR related function $f_{CSR} = C_3 \cdot CSR^{C_4 \cdot N^{C_5}}$	C_3	0.031
	C_4	1.715
	C_5	-0.100
α related function $f_\alpha = \left(C_6 \ln N + C_7\right) \cdot \alpha$	C_6	-0.0013
	C_7	0.0043

371

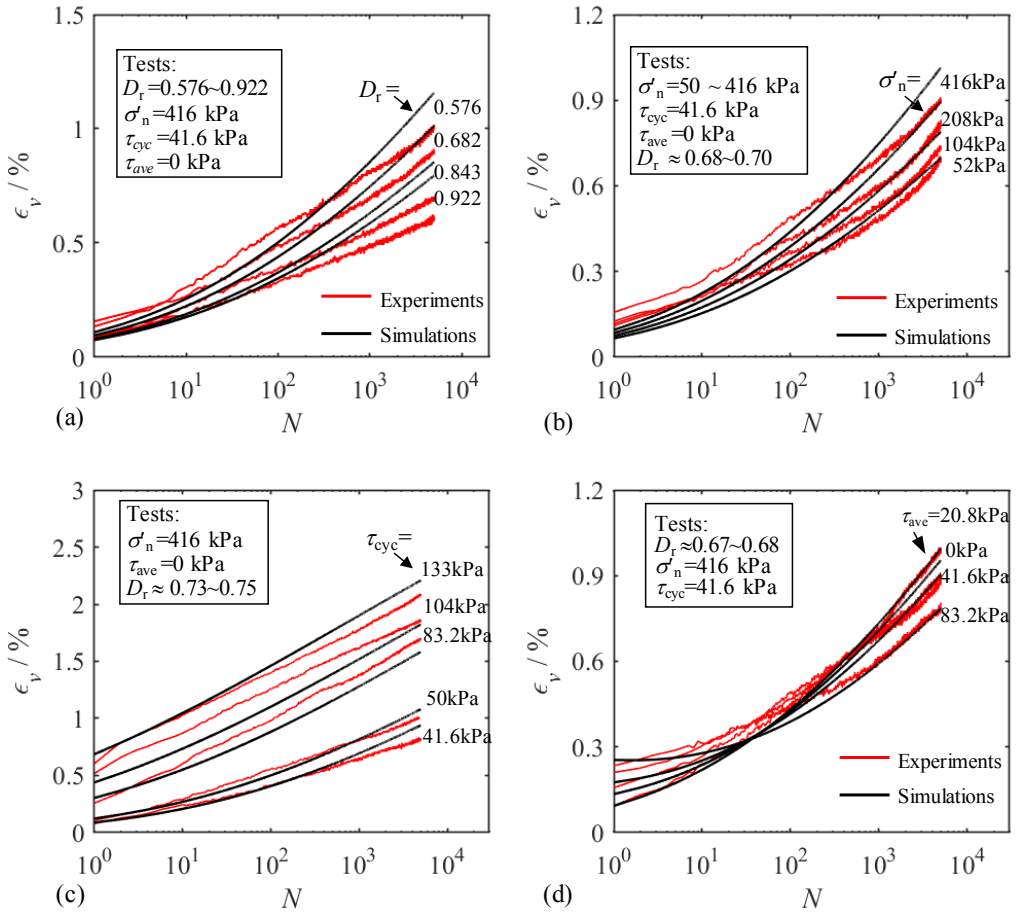

Figure 7 Performance of analytical model: (a) calibration with different relative densities; (b) calibration with different effective normal stresses; (c) calibration with different cyclic shear stress; (d) calibration with different average shear stress

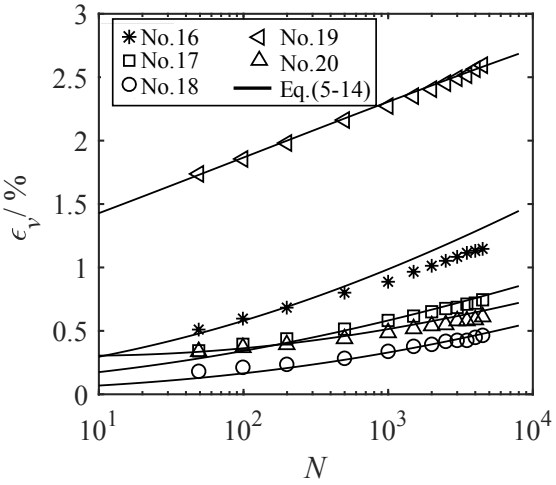

Figure 8 Validation of the analytical model by five additional tests No.16-20

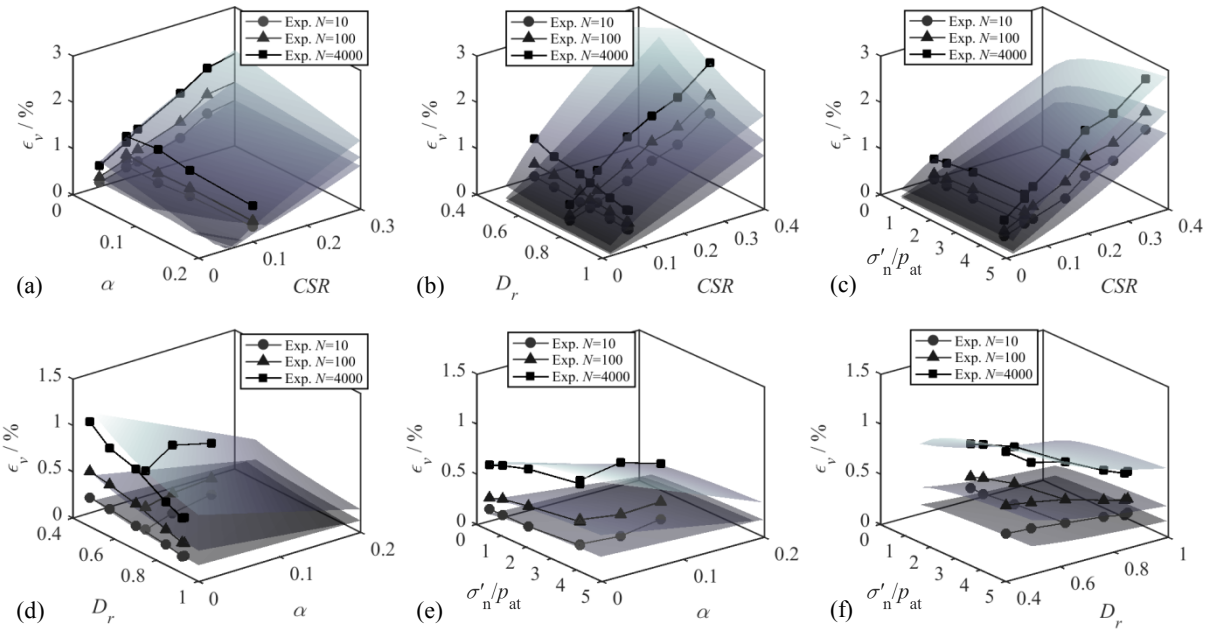

Figure 9 Volumetric strain accumulation evolution with 10, 100 and 4000 cycles for different effects of (a) α and CSR, (b) D_r and CSR, (c) σ'_n/p_{at} and CSR, (d) D_r and α, (e) σ'_n/p_{at} and α and (f) σ'_n/p_{at} and D_r

5 Discussion

Herein, Fontainebleau sand NE34, as a geotechnical reference siliceous material, has been selected to develop an analytical model of cyclic strain accumulation accounting for important factors [25, 47, 48, 51]. The simple shear tests for various factors are designed according to the deformation behaviour of soil element around the pile [5, 7, 20]. the cyclic experimental results show that the regularly volumetric strain accumulates under different initial states, and the interpretation of results indicates that the effects of the four key factors can be respectively formulated through a simple expression Eq. (15). The results about the effects of cyclic shear stress ratio and initial relative density on the strain accumulation are also consistent with Nikitas et al. [46], which emphasise the cyclic degradation behaviour. The analytical model Eq. (15) was proposed based on stress-controlled simple shear tests which can be control by stress amplitude and can well simulate the cyclic loading condition in offshore engineering.

This is different from the strain degradation model of Wichtmann et al. [18] focusing on the effects of strain amplitude coupling with other factors since their tests were strain-controlled.

A multi-dimensional sensitivity analysis was performed based on the analytical model. As shown in Figure 9, the accumulation of volumetric strain is greatly enhanced by CSR and resisted by average shear stress. The most sensitive combined group is the combination of D_r and CSR. The least sensitive combined group is the combination of D_r and σ'_n.

It should be pointed out that, the developed analytical equations are also applicable for other types of tests (e.g. triaxial tests, direct shear tests and hollow cylinder tests), and the prerequisite can be based on the owning parameters calibrated from their respective tests. Note that, it is also possible to extend the proposed model to general stress space after being calibrated by different types of tests implying different stress conditions. In this sense the proposed model is an important base.

6 Conclusion

This work is focused on an investigation of the strain accumulation behaviour of a soil element subjected to a long-term cyclic loading under drained simple shear condition, which can be used to interpret the cyclic strain accumulation of soil adjacent to the pile. To achieve this objective, certain key conclusions were drawn:

1) The constant normal stress cyclic simple shear tests can replicate the key response of cyclic strain accumulation considering different initial states, namely relative density (D_r), normal stress (σ'_n), cyclic shear stress (*CSR*) and average shear stress (α). The strain accumulation is highly sensitive to the state of *CSR*, with a larger magnitude of CSR (more than 0.2) resulting in a larger level of densification. The most sensitive factors followed are D_r and σ'_n, and for Fontainebleau sand the

magnitudes of D_r = 39% (loose sand) and σ'_n = 416 kPa correspond to relatively large densification potential. Moreover, a low magnitude of α (e.g. α = 0.05) can restrain the densification.

1) The interpretation of experimental results indicates that the accumulation of volumetric strain is effected by four initial states (D_r, σ'_n, *CSR*, α), which was used to formulate four key factors related equation.

3) An analytical model of volumetric strain accumulation was developed, considering the abovementioned four effects. The parameters can be calibrated based on training tests. The applicability of the model was validated by predicting the remainder of the tests with the calibrated parameters.

This work focused on the study of four factors (initial void ratio, initial normal stress, cyclic shear stress and average shear stress) on the volumetric strain developed during cyclic loading, which will be extended for other influencing factors (the characteristics of phase transformation, drainage dependence, saturation, frequency etc.). Future work will focus on extending the 1-D equation to a model with full tensor.

Note that Fontainebleau sand NE34 is a very well-known and widely adopted geotechnical reference siliceous sand, and thus the results achieved in this study is representative. But other standard sand will be adopted for tests in the near future to further validate the behaviour and the model performance.

Acknowledgements

This research was financially supported by the Key Special Project for Introduced Talents Team of Southern Marine Science and Engineering Guangdong Laboratory (Guangzhou) (No.: GML2019ZD0503) and the Research Grants Council (RGC) of Hong Kong Special Administrative Region Government (HKSARG) of China (Grant No.: PolyU R5037-18F).

References

[1] Lehane B, Jardine R, Bond AJ, Frank R. Mechanisms of shaft friction in sand from instrumented pile tests. Journal of Geotechnical Engineering. 1993;119:19-35.

[2] Jardine R, Chow F, Overy R, Standing J. ICP design methods for driven piles in sands and clays: Thomas Telford London; 2005.

[3] Li S, Zhang Y, Jostad HP. Drainage conditions around monopiles in sand. Applied Ocean Research. 2019;86:111-6.

[4] Jardine R, Standing J. Pile load testing performed for HSE cyclic loading study at Dunkirk, France: Great Britain, Health and Safety Executive; 2000.

[5] Jardine R, Standing J. Field axial cyclic loading experiments on piles driven in sand. Soils and foundations. 2012;52:723-36.

[6] Tsuha CdHC, Foray P, Jardine R, Yang Z, Silva M, Rimoy S. Behaviour of displacement piles in sand under cyclic axial loading. Soils and Foundations. 2012;52:393-410.

[7] Rimoy SP. Ageing and axial cyclic loading studies of displacement piles in sands. Imperial College London. 2013.

[8] Bekki H, Tali B, Canou J, Dupla J-C, Bouafia A. Influence of the cyclic loading of very large number of cycles on the pile capacity. Journal of Applied Engineering Science & Technology. 2016;2:51-5.

[9] Kerner L, Dupla J-C, Cumunel G, Argoul P, Canou J, Pereira J-M. Experimental Study on a Scaled Model of Offshore Wind Turbine on Monopile Foundation. Models, Simulation, and Experimental Issues in Structural Mechanics: Springer; 2017. p. 249-67.

[10] Le Kouby A, Dupla JC, Canou J, Francis R. The effects of installation order on the response of a pile group in silica sand. Soils and Foundations. 2016;56:174-88.

[11] Zhao H-Y, Jeng D-S, Liao C-C, Zhang J-S, Guo Z, Chen W-Y. Numerical modelling of liquefaction in loose sand deposits subjected to ocean waves. Applied Ocean Research. 2018;73:27-41.

[12] Wang J, Jiang M. Unified soil behavior of interface shear test and direct shear test under the influence of lower moving boundaries. Granular Matter. 2011;13:631-41.

[13] Wu H-N, Shen S-L, Liao S-M, Yin Z-Y. Longitudinal structural modelling of shield tunnels considering shearing dislocation between segmental rings. Tunnelling and Underground Space Technology. 2015;50:317-23.

[14] Shen S-L, Cui Q-L, Ho C-E, Xu Y-S. Ground response to multiple parallel microtunneling operations in cemented silty clay and sand. Journal of Geotechnical and Geoenvironmental Engineering. 2016;142:1-12.

[15] Xiong H, Nicot F, Yin Z. From micro scale to boundary value problem: using a micromechanically based model. Acta Geotechnica. 2019;14:1307-23.

[16] Xiong H, Nicot F, Yin ZY. A three-dimensional micromechanically based model. International Journal for Numerical Analytical Methods in Geomechanics. 2017;41:1669-86.

[17] Yang J, Yin Z-Y, Liu X-F, Gao F-P. Numerical analysis for the role of soil properties to the load transfer in clay foundation due to the traffic load of the metro tunnel. Transportation Geotechnics. 2020;23:1-12.

[18] Wichtmann T, Niemunis A, Triantafyllidis T. Strain accumulation in sand due to cyclic loading: drained triaxial tests. Soil Dynamics and Earthquake Engineering. 2005;25:967-79.

[19] Coop M, López-Querol S. Drained cyclic behaviour of loose Dogs Bay sand. Géotechnique. 2012;62:281-9.

[20] Sim WW, Aghakouchak A, Jardine RJ. Cyclic triaxial tests to aid offshore pile analysis and design. 2013.

[21] Mamou A, Powrie W, Priest J, Clayton C. The effects of drainage on the behaviour of railway track foundation materials during cyclic loading. Géotechnique. 2017:1-10.

[22] Sun Q, Cai Y, Chu J, Dong Q, Wang J. Effect of variable confining pressure on cyclic behaviour of granular soil under triaxial tests. Canadian Geotechnical Journal. 2017;54:768-77.

[23] Jiang M, Harris D, Zhu H. Future continuum models for granular materials in penetration analyses. Granular Matter. 2007;9:97-108.

[24] Boulon M, Foray P. Physical and numerical simulation of lateral shaft friction along offshore piles in sand. Proceedings of the 3rd International Conference on Numerical methods in Offshore piling, Nantes, France1986. p. 127-47.

[25] Pra-ai S, Boulon M. Soil–structure cyclic direct shear tests: a new interpretation of the direct shear experiment and its application to a series of cyclic tests. Acta Geotechnica. 2017;12:107-27.

[26] Anderson K. Bearing capacity under cyclic loading-offshore, along the coast, and on land. Canadian Geotechnical Journal. 2009;46:513-35.

[27] Vaid Y, Stedman J, Sivathayalan S. Confining stress and static shear effects in cyclic liquefaction. Canadian Geotechnical Journal. 2001;38:580-91.

[28] Matsuda H, Hendrawan AP, Ishikura R, Kawahara S. Effective stress change and post-earthquake settlement properties of granular materials subjected to multi-directional cyclic simple shear. Soils and Foundations. 2011;51:873-84.

[29] Da Fonseca AV, Soares M, Fourie A. Cyclic DSS tests for the evaluation of stress densification effects in liquefaction assessment. Soil Dynamics and Earthquake Engineering. 2015;75:98-111.

[30] Porcino D, Marcianò V, Granata R. Cyclic liquefaction behaviour of a moderately cemented grouted sand under repeated loading. Soil Dynamics and Earthquake Engineering. 2015;79:36-46.

520 [31] Çellek S. Comparison of Grain Size Distribution and Grain Shape of Various Sand
521 Samples. Geotechnical and Geological Engineering. 2019;37:5019-33.

522 [32] Ng CWW, Choi CE, Liu LHD, Wang Y, Song D, Yang N. Influence of particle size on
523 the mechanism of dry granular run-up on a rigid barrier. Géotechnique Letters. 2017;7:79-89.

524 [33] Cabalar AF. Inuence of grain shape and gradation on the shear behavior of sand mixtures.
525 Scientia Iranica. 2017;25:3101-9.

526 [34] Li Y. Effects of particle shape and size distribution on the shear strength behavior of
527 composite soils. Bulletin of Engineering Geology and the Environment. 2013;72:371-81.

528 [35] Ghadr S, Assadi-Langroudi A. Effect of Grain Size and Shape on Undrained Behaviour
529 of Sands. International Journal of Geosynthetics and Ground Engineering. 2019;5:18.

530 [36] Cabalar AF. Cyclic behavior of various sands and structural materials interfaces.
531 Geomechanics and Engineering. 2016;10:1-19.

532 [37] Cabalar AF, Dulundu K, Tuncay K. Strength of various sands in triaxial and cyclic direct
533 shear tests. Engineering Geology. 2013;156:92-102.

534 [38] Silver ML, Seed HB. Deformation characteristics of sands under cyclic loading. Journal
535 of Soil Mechanics & Foundations Div. 1971.

536 [39] Silver ML, Seed HB. Volume changes in sands during cyclic loading. Journal of Soil
537 Mechanics & Foundations Div. 1971.

538 [40] Youd TL. Compaction of sands by repeated shear straining. Journal of Soil Mechanics &
539 Foundations Div. 1972;98.

540 [41] Ghayoomi M, McCartney JS, Ko H-YJJog, engineering g. Empirical methodology to
541 estimate seismically induced settlement of partially saturated sand. 2013;139:367-76.

542 [42] Kaggwa WS, Booker JR, Carter J. Residual strains in calcareous sand due to irregular
543 cyclic loading. Journal of geotechnical engineering. 1991;117:201-18.

544 [43] Duku PM, Stewart JP, Whang DH, Yee E. Volumetric strains of clean sands subject to
545 cyclic loads. Journal of geotechnical and geoenvironmental engineering. 2008;134:1073-85.

546 [44] Shen S-L, Wang Z-F, Yang J, Ho C-E. Generalized approach for prediction of jet grout
547 column diameter. Journal of Geotechnical and Geoenvironmental Engineering.
548 2013;139:2060-9.

549 [45] Shen S-L, Wu Y-X, Misra A. Calculation of head difference at two sides of a cut-off
550 barrier during excavation dewatering. Computers and Geotechnics. 2017;91:192-202.

551 [46] Nikitas G, Arany L, Aingaran S, Vimalan J, Bhattacharya S. Predicting long term
552 performance of offshore wind turbines using cyclic simple shear apparatus. Soil Dynamics and
553 Earthquake Engineering. 2017;92:678-83.

554 [47] Dupla J, Canou J. Caractérisation mécanique du sable de Fontainebleau apartir d'essais
555 triaxiaux de compression et d'extension. Rapport Interne CLOUTERRE II, CERMES–ENPC.
556 1994.

557 [48] Andria-Ntoanina I, Canou J, Dupla J. Caractérisation mécanique du sable de
558 Fontainebleau NE34 à l'appareil triaxial sous cisaillement monotone. Laboratoire Navier–
559 Géotechnique CERMES, ENPC/LCPC. 2010.

560 [49] Aghakouchak A, Sim WW, Jardine RJ. Stress-path laboratory tests to characterise the
561 cyclic behaviour of piles driven in sands. Soils and Foundations. 2015;55:917-28.

562 [50] Taiba AC, Mahmoudi Y, Belkhatir M, Schanz T. Experimental Investigation into the
563 Influence of Roundness and Sphericity on the Undrained Shear Response of Silty Sand Soils.
564 Geotechnical Testing Journal. 2018;41:619-33.

565 [51] Wu Z-X, Dano C, Hicher P-Y, Yin Z-Y. Estimating normal effective stress degradation
566 in sand under undrained simple shear condition. European Journal of Environmental Civil
567 Engineering. 2018:1-20.

568 [52] Bjerrum L, Landva A. Direct simple-shear tests on a Norwegian quick clay. Geotechnique.
569 1966;16:1-20.

570 [53] Hooker P. The development of automated testing in geotechnical engineering. Proceeding
571 of the Indian Geotechnical Conference2002. p. 96-102.

572 [54] Vaid YP, Negussey D. Relative density of pluviated sand samples. Soils and Foundations.
573 1984;24:101-5.

574 [55] Yang Z, Jardine RJ, Zhu B, Foray P, Tsuha CdHC. Sand grain crushing and interface
575 shearing during displacement pile installation in sand. Géotechnique. 2010;60:469-82.

576 [56] Yang Z, Wu Y. Critical state for anisotropic granular materials: a discrete element
577 perspective. International Journal of Geomechanics. 2017;17:1-12.

578 [57] Cui L, Bhattacharya S. Soil–monopile interactions for offshore wind turbines. Proceedings
579 of the Institution of Civil Engineers-Engineering Computational Mechanics. 2016;169:171-82.

580 [58] Lentz R, Baladi G. Simplified procedure to characterize permanent strain in sand subjected
581 to cyclic loading. International Symposium on soils under cyclic and transient loading1980. p.
582 89-95.

583

584 **Figure captions**

585 Figure 1 Analysis of soil element based on simple shear apparatus

586 Figure 2 Summary of drained cyclic simple shear results: (a)-(b) comparisons by different
587 initial relative densities; (c)-(d) comparisons by different effective normal stresses;
588 (e)-(f) comparisons by different cyclic shear stress ratios and (g)-(h) comparisons by
589 different average shear stress ratios.

590 Figure 3 Volumetric strain accumulation with different relative densities: (a) volumetric strain
591 versus number of cycles; (b) volumetric strain versus relative density; (c) reference
592 volumetric strain versus number of cycles

593 Figure 4 Volumetric strain accumulation with different normal stress level: (a) volumetric
594 strain versus number of cycles; (b) volumetric strain versus normal stress level; (c)
595 reference volumetric strain versus number of cycles

596 Figure 5 Volumetric strain accumulation with different cyclic stress ratio: (a) volumetric strain
597 versus number of cycles; (b) normalized volumetric strain versus cyclic shear stress
598 ratio; (c) reference volumetric strain versus number of cycles

599 Figure 6 Volumetric strain accumulation with different average shear stress ratio: (a)
600 volumetric strain versus number of cycles; (b) normalized volumetric strain versus
601 average shear stress ratio; (c) reference volumetric strain versus number of cycles

602 Figure 7 Performance of analytical model: (a) calibration with different relative densities; (b)
603 calibration with different effective normal stresses; (c) calibration with different cyclic
604 shear stress; (d) calibration with different average shear stress

605 Figure 8 Validation of the analytical model by five additional tests No.16-20

606 Figure 9 Volumetric strain accumulation evolution with 10, 100 and 4000 cycles for different
607 effects of (a) α and CSR, (b) D_r and CSR, (c) σ'_n/p_{at} and CSR, (d) D_r and α, (e) σ'_n/p_{at}
608 and α and (f) σ'_n/p_{at} and D_r

609